HAL
open science

In situ spectroscopic ellipsometry monitoring of diamond multilayers grown by microwave plasma enhanced chemical vapor deposition

J. Bousquet, F. Jomard, E. Bustarret, D. Eon

To cite this version:

J. Bousquet, F. Jomard, E. Bustarret, D. Eon. In situ spectroscopic ellipsometry monitoring of diamond multilayers grown by microwave plasma enhanced chemical vapor deposition. Diamond and Related Materials, 2018, 86, pp.41 - 46. 10.1016/j.diamond.2018.04.009 . hal-01931490

HAL Id: hal-01931490

https://hal.science/hal-01931490v1

Submitted on 27 Nov 2018

HAL is a multi-disciplinary open access archive for the deposit and dissemination of scientific research documents, whether they are published or not. The documents may come from teaching and research institutions in France or abroad, or from public or private research centers.

L'archive ouverte pluridisciplinaire **HAL**, est destinée au dépôt et à la diffusion de documents scientifiques de niveau recherche, publiés ou non, émanant des établissements d'enseignement et de recherche français ou étrangers, des laboratoires publics ou privés.

In situ Spectroscopic Ellipsometry monitoring of diamond multilayers grown by Microwave Plasma Enhanced Chemical Vapor Deposition

J. Bousquet[1,2*], F. Jomard[3], E. Bustarret[1,2], D. Eon[1,2]

[1] *Univ. Grenoble Alpes, Inst. NEEL, F-38042 Grenoble, France*

[2] *CNRS, Inst. NEEL, F-38042 Grenoble, France*

[3] *GEMaC, UVSQ and CNRS, 45, avenue des Etats Unis, 78035 Versailles, France*

Abstract:

Thanks to its unique properties, diamond is intensively investigated for the development of optical and electronic devices. These applications, such as pseudo-vertical Schottky diodes or Bragg mirrors, rely on the synthesis of boron-doped (p_+) and non-intentionally doped (*nid*) stacked epilayer with well-controlled thicknesses, doping level and sharp interfaces. Such structures require a time-consuming optimization of the growth processes throughout the use of destructive techniques such as Secondary Ion Mass Spectroscopy (SIMS), Transmission Electron Microscopy (TEM) or transport measurements. From this perspective, the use of an *in situ* characterization tool is a considerable asset.

In this paper, we demonstrate that spectroscopic ellipsometry, implemented to be used *in situ* during the Plasma Enhanced Chemical Vapor Deposition (MPCVD) process, is a powerful and non-destructive technique to characterize diamond based devices. Moreover, it can also be sensitive enough to access the gas flow dynamics in the reactor. To this aim, two doped and *nid* multilayer stack have been investigated. The doping profile of a doped layer, extracted from the optical spectra is compared to the one obtained by SIMS and the growth rate of *nid* epilayers grown under various flow rate, is derived based on this technique.

[*] Jessica Bousquet jessica.bousquet12@gmail.com +33(0)674038520

1. Introduction

The fabrication of diamond-based power or optical devices such as n/i/p and Schottky pseudo-vertical diodes [1-3] or Bragg mirror [4,5], requires the growth of boron-doped and intrinsic diamond layers with steep interfaces, well-controlled thicknesses and doping level. In most cases, an optimization of the growth conditions is needed, requiring the growth of a large number of samples and the use of destructive and time-consuming techniques such as Secondary Ion Mass Spectroscopy (SIMS) or Transmission Electron Microscopy (TEM).

In situ spectroscopic ellipsometry has already been reported to be an efficient way to characterize the nucleation and coalescence of polycrystalline diamond grown on silicon thanks to the substantial index contrast between the two materials [6-12]. However, in spite of several papers [13,14] indicating a significant decrease of the refracting index in doped epilayers induced by free holes absorption in the infrared region, very few studies were undertaken to characterize diamond single crystal by using *ex situ* spectroscopic ellipsometry. And all of them concern pristine semi-infinite layers [15,16]. Thus, contrary to a large number of materials, the very first *ex situ* measurement to precisely assess the thickness and doping level of boron doped diamond monolayers was only demonstrated in 2013 [17]. Recently, the same technique has been used *in situ* on the reactor to monitor in real time the fabrication of Bragg mirrors [5].

This paper aims at going one step further by showing that substantial information can be extracted from an on-line treatment of the spectra recorded during the growth of p^+ or *nid* diamond layers. First, we show that a proper free carrier concentration depth profile of a metallic heavily boron doped (p^+) layer can be deduced from *in situ* spectra by comparing our measurements with SIMS profiles. Then, the sensitivity of the technique is assessed. By studying the transient regime of the growth of a stack of *nid* epilayers synthetized under various gas flow rates we will also demonstrate that this technique can give access to the transit time of gases inside the reactor, a considerable asset for the elaboration of new growth recipes for thin film such as boron [18,19] or nitrogen delta-doped layers [20].

2. Experimental

2.1. Sample preparation

All samples were grown by MPCVD in a vertical silica tube NIRIM type reactor on 3x3 mm^2 and [100]-oriented diamond substrates (purchased from Sumitomo Electric). Prior to each growth, pure hydrogen plasma was performed to stabilize the temperature and the pressure inside the chamber. Then a *nid* buffer layer was grown by injecting a H_2+CH_4 gas mixture. The microwave power was adjusted at 280 W to keep a surface temperature around 910°C as measured by a pyrometer, and the metallic layers were synthetized at 830°C by adding B_2H_6 to the gas mixture. The growth conditions of the p^+ layer and the *nid* epilayer stacks are detailed in table 1.

A thick doped layer ([B]>10^{17} cm^{-3}), covered by a *nid* film, was grown on each substrate to get a sufficient index contrast. Acting as a mirror, this p^+ is needed to measure the second *nid* layers (for the *nid* stack case) and can be used to increase the sensitivity of the measurement by maximizing the amplitude of the reflected beamlight in the first experiment (*p*+ doping profile assessment).

	Pressure (torr)	**CH_4/H_2 (%)**	**B/C (ppm)**	**Gas flow rate (sccm)**	**Growth time (min)**
p^+	33	3.54	2000	100	7
***nid* stack**	50	1	0	70, 100, 150, 200 and 1000, 1500, 2000	1.5 and 1

Table 1 : Details of the growth conditions of the metallic sample and the nid epilayer stack.

2.2.Secondary Ion Mass Spectroscopy

The SIMS measurements were performed in a CAMECA IMS7F system with collection of a negative secondary ^{11}B and ^{12}C ions or their compounds. A O_2^+ primary ions beam at 5 keV, reduced to 0.5 keV for thin layers, was used.

2.3.Spectroscopic Ellipsometry

In Spectroscopic Ellispometry, the change of the polarization state of the beam light is measured throughout the two ellipsometric angles ψ and Δ which are defined by the ratio ρ of the two complex reflection coefficients as followed [21]:

$$\rho = \frac{r_p}{r_s} = \tan(\psi)\exp(i\Delta) \quad (1)$$

With r_p and r_s the complex reflection coefficients for the electric field which are respectively parallel and perpendicular to the incidence plane.

Our *in situ* measurements were performed over a spectral range of 210-1690 nm, with a J. A. Woolam M2000 ellipsometer running under the Compleate Ease software. The source and the detector were placed on each side of the quartz tube and aligned with the sample so that the polarized beam light coming through the silica tube via the waveguide slits is reflected by the sample toward the center of the detector with an angle of around 75° (see Fig. 1a). Note that the overall surface of the sample impacted by the beam light is about 2.4x4 mm^2 *i.e.* along the sample diagonal. All optical measurements are thus averaged over the surface of the sample.

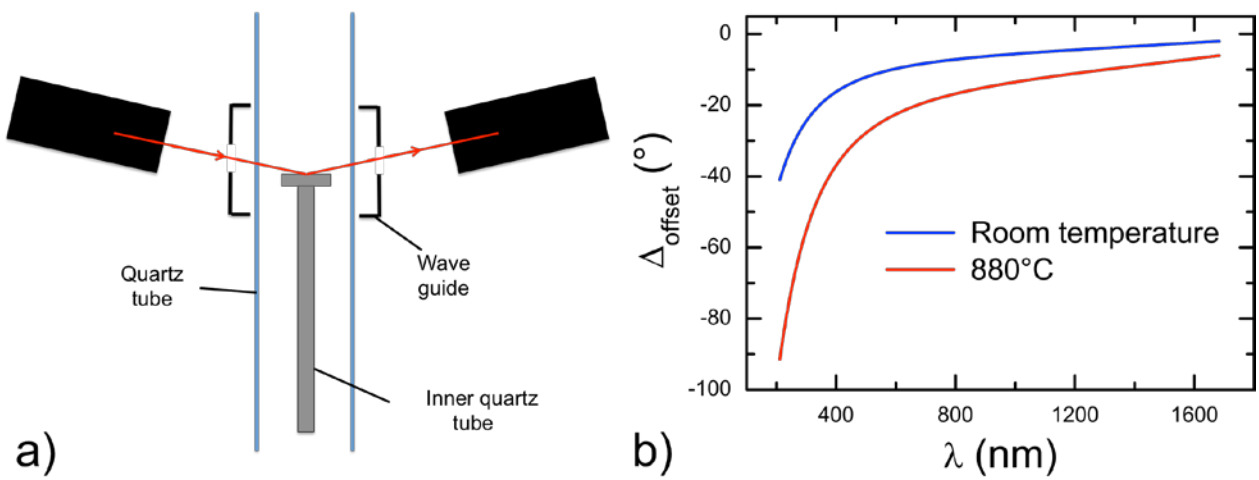

Figure 1 a) Schematic of the experimental setup used for in situ measurement. b) Spectral dependence of the Δ angle offset at room temperature and at 880°C during the H_2 plasma.

The *in situ* configuration requires considering the influence of the different interfaces crossed by the beam light (here the silica tube) but also of the temperature on the ellipsometric angles. To that aim, the same protocol was followed before each growth. First, an *ex situ* spectrum of the substrate was recorded and modeled. Then, a second measurement was carried out *in situ* at room temperature. A shift of the Δ angle, induced by the silica tube, was then estimated from the

comparison of the two spectra. This shift, presented in blue in figure 1.b, was taken into account by adding the "Prism" function of the software (4 parameters Cauchy formula) to the model defined from the *ex situ* spectrum. The same procedure was followed during the hydrogen plasma at around 880°C. For all *in situ* measurements, a strong shift of Δ has been observed whereas almost no change in the spectral dependence of ψ could be noticed tending to indicate that the influence of the temperature on the dielectric constants of the substrate is negligible in comparison to the transmittance change induced by the silica tube heating. Thus, at this stage, the new Δ offset is taken into account by fitting the new spectrum and adjusting the 4 parameters previously introduced (see red curve in Figure 1.b). Note that a final spectral dependence of the Δ shift, quite similar whatever the substrate, has been observed, pointing again to the quartz tube as a possible origin for this shift.

As mentioned elsewhere [5], the substrate, considered as a semi-infinite medium, and the *nid* diamond layers of finite thickness, could be simulated by a Cody-Lorentz model. In this latter one, the direct E'_0 and indirect E_g^{ID} band gap absorptions of diamond were simulated by fixing the energy of the principal oscillator at 7.3 eV and adjusting the amplitude and the tail of the Lorentzian contribution whereas the E_2 peak absorption was taken into account by fixing the UV Pole energy at 11 eV.

A Drude component (ε_{Drude}) was added to this UV oscillator (ε_{nid}) in order to model the boron-doped samples. The thickness of the epilayer was extracted from the spectral oscillation of the ellipsometric angles. The electronic properties were deduced from the modeling of the optical absorption at low energy using two independent sets of parameters; respectively the resistivity at zero frequency (ρ_0) and the scattering time (τ_{opt}), or the renormalized free carrier concentration (N_{opt}/m_{opt}^*) and mobility (μ_{opt}).

Since our previous report [17] the spectral range of our ellipsometer has been extended allowing a more accurate extraction of the holes effective mass. The recent comparison of the optical parameters with SIMS and transport measurements gave a new effective mass of around $m^*=0.4\ m_0$ (with m_0 the electron mass), within the error bar of the previous value.

Considering 3 bands degenerated at the Γ point, the total density of state effective mass can be approximated by the expression

$$m_{opt}^* = \frac{m_{hh}^{3/2}+m_{lh}^{3/2}+m_{so}^{3/2}}{m_{hh}^{1/2}+m_{lh}^{1/2}+m_{so}^{1/2}} \qquad (2)$$

m_{hh}, m_{lh} and m_{so} being the effective masses of the heavy, light and spin-orbit holes in the

diamond band structure. This value of 0.4 m_0 is thus in good agreement with the recent measurements by electron cyclotron resonance (m^*_{opt}=0.47m_0) [22] and Angle Resolved Photoemission Spectroscopy (m^*_{opt}=0.41m_0) [23] but also with earlier LMTO calculation of Willatzen [24] (m^*_{opt}=0.45m_0) or Eremets [25]. Note that our value is however lower than the one predicted by other earlier works [26-28].

3. Results

3.1.Boron-doped layer

On top of providing real-time feedbacks from the layer properties, the use of *in situ* Spectroscopic Ellipsometry enable an easy extraction of its doping profile without the need of a complex model.

In the following example, the p^+ epilayer of a multilayer stack was measured in real time by recording one spectrum every 2.4 s. After the growth of a *nid* epilayer, the metallic film was deposited during 7 minutes under the conditions detailed in table 1. Then, a short rinsing hydrogen plasma was used before capping with a *nid* film and continuing the growth with further layers. The spectral variation of the ellipsometric angles, recorded at three different growth times, are presented in figure 2.

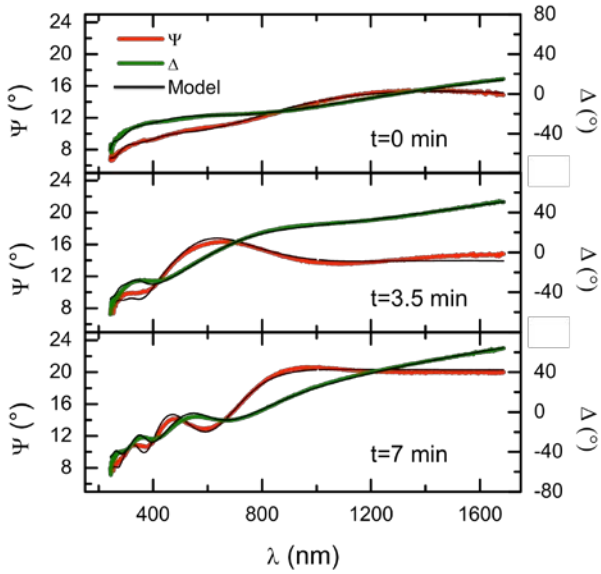

Figure 2: Spectral variation of the ellipsometric angles recorded at t=0, 3.5 and 7 min. The black lines correspond to the model "a" (discussed in section 2.3 and figure 4). The overall mean square deviation of the fitting (MSE) is situated between 6 and 10 whatever the model.

In the first spectrum, recorded before the growth, a Δ angle of 15° can be observed above 166 nm. This value, higher than the one expected in pristine diamond (Δ=0°), is due to the infrared absorption induced by free carries of the underlying mirror layer. Note that an increase of the Δ angle from 15° to 63° at 7min, together with a decrease of the Fabry-Perot fringes periodicity from 345 to 145 nm between the two last spectra, confirms the increasing thickness of the absorbing layer.

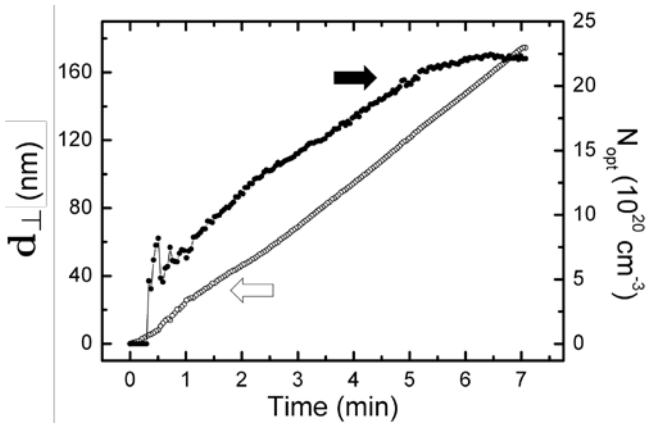

Figure 3: Time dependence of the thickness (open circles) and optical carrier concentration (full circles) of the doped layer. The data are extracted from the spectra recorded in real time during the growth using the Model a (in blue in Figure 4).

The thickness $d_\perp$ and the optical free carrier concentration N_{opt}, extracted from the real-time fitting of each spectrum and assuming an effective mass of $0.4m_0$ is presented in Figure 3.

As expected, the thickness increases linearly with time and with a growth rate of around 26 $nm.min^{-1}$. More strikingly, the optical carrier concentration increases as well. As confirmed by the SIMS profiles, presented in figure 4, the doping is not homogeneous over the growth axis and increases with the thickness of the film. We can also observe that during the first 30 s of the growth, N_{opt} stays at zero before jumping directly to around 5.10^{20} cm^{-3}. Indeed, within this time lapse, the boron incorporation increases with $d_\perp$. But, to fit properly the optical spectra a model including a Drude component, an infrared absorption, induced by a minimum of free carrier concentration is required. Note that the detection limit obtained here is situated within the region of the Metal-to-Insulator transition [29-31].

In the upper panel of Figure 4, the doping profile $N_{opt}(d_{\perp})$ of the film, is compared to three SIMS profiles performed in different areas of the sample. To do so, the optical data have been flipped and shifted to coincide with the SIMS profile. We estimated the position of top layer interface as the depth where the Boron concentration start to decrease and used the value of 656 nm as the reference to position the optical points.

As detailed in the lower panel, the optical profiles have been simulated using different models for the underlying layers (*nid* over p^+). In blue, each of them is taken into account whereas in purple, the overall optical response is simulated by an *ad hoc* mathematical function. Compared to the model a, this latter one enable a fast and perfect reproduction of the spectrum but has no real physical meaning. However, we can notice that whatever the model used, and considering a full activation of the boron atoms, the boron profile can be faithfully reproduced by spectroscopic ellipsometry. Note that even if the two optical profiles are situated within the bounds of the three SIMS measurements, a small difference of thickness is noticed. This latter one is smaller than 10 nm and could be attributed to thickness inhomogeneities across the layer surface, but also to the uncertainty of the SIMS sputtered thickness measurement itself. Note also that the reconstruction of the falling edge of the layer from the spectra (at around 656 nm in depth) cannot be undertaken because of the post-hydrogen process.

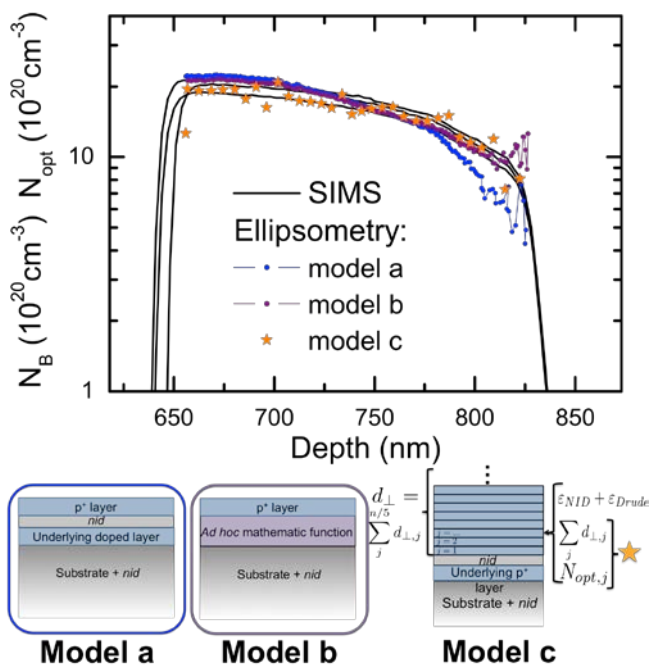

Figure 4 Upper panel: Comparison between the optical carrier profiles reconstructed with three different models and the boron profile deduced from SIMS measurements (black lines). To enable

this comparison, the optical data have been flipped and shifted to coincide with the SIMS profile depth; bottom and top layer interfaces situated around 830 nm and 656 nm. Lower panel: Schematic of the optical models used for the spectra fitting. Model a (in blue) each underlying layer is taken into account. Model b (in purple) the p^+ and nid underlying layers are modeled together by an ad hoc mathematic function. Model c (in orange) the p+ layer is divided in n sub multi-layers. 5n being the total number of spectra recording during the growth.

It has to be stressed that optical and SIMS profiles cannot be rigorously compared if the doping level of the layer is not perfectly homogeneous along the growth axis. Indeed, at time t, and despite absorption, the entire layer is probed by the ellipsometer and the extracted parameters are thus averaged over the whole layer thickness. In the present case, where the boron concentration seems to increase with $d_{\perp}$, the N_{opt} reported are thus under-estimated compared to their local values. To solve this problem, a new profile has been deduced *a posteriori* from a third model (model c in Figure 4). Starting from the model a, the doped layer were divided into several sub-layers with $d_{\perp,j}$, $N_{opt,j}$ and $\mu_{opt,j}$ as free parameters. In order to limit the computing time, one sub-layer corresponds to the diamond grown over 12s (5 spectra). The corresponding free carrier concentration (orange stars), reported as a function of the cumulated thicknesses of all sub-layers, presents some local inhomogeneities but is in fair agreement with the SIMS and is quite close to the first two optical profiles. We can conclude that in the present case, where the boron incorporation increase with the layer thickness, the models introduced previously were much more efficient and less time consuming.

3.2.Non-Intentionally doped layer

Beside the doping profile, the analysis of spectra recorded *in situ* during growth can also provide some information about the dynamic of the gas flow. The synthesis of the *nid* stack, detailed in table 1, has been recorded using a fast acquisition mode (one record every 0.54 s). The total gas flow rate φ was varied from 70 to 2000 sccm. In order to study the very first steps of the *nid* growth, two pure hydrogen plasmas, with the same total flow rate than that of the *nid*, have been performed before and after each growth. The time-dependence of the optical thicknesses of each layer is displayed in Figure 5.

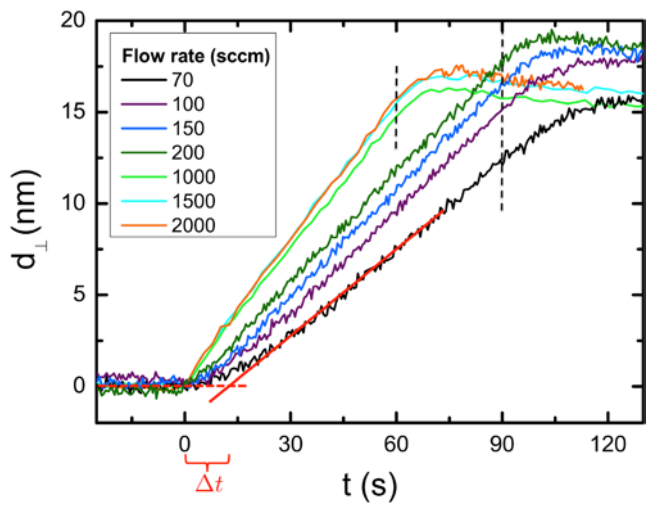

Figure 5. Evolution of the optical thickness of the nid layers grown under various gas flow rate. The gas mixture (H_2+CH_4) is injected at t=0 s until a new H_2 plasma process (represented by the vertical dashed lines). As an example, the steady state (H_2 plasma) and the permanent regime of the 70 sccm layer are highlighted by the red lines, respectively dashed and continued lines.

During the H_2 plasma, $d_\perp$ is constant and can be modeled by the red dashed line. After the methane injection at t=0s, $d_\perp$ begins to increase until reaching a permanent regime (solid line). The characteristic delay time Δt of the transient regime can be defined as the time elapsed between t_{inj} and the crossing point of the two red lines.

As displayed in Figure 6, the growth rate (slope of the permanent regime) of the different layers increases rapidly with φ and starts to saturate around 1000-1500 sccm.

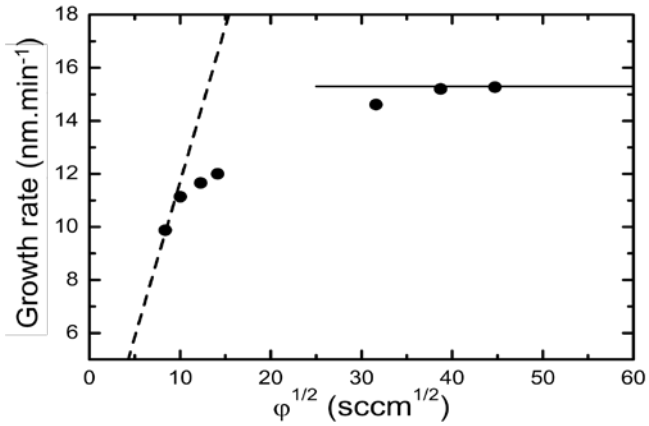

Figure 6. Layer growth rate, deduced from fig. 5 as a function of the square root of the gas flow rate. The dashed and continuous lines correspond to the mass transport limited and surface reaction limited regime, respectively.

A similar dependence has been reported on nanocristalline HFCVD diamond films [32] but never been detailed so far. The growth mechanisms of diamond are not perfectly understood and include a large number of reactions that can all be modified by the gas flow rate or the flow regime. This latter one might also be turbulent under 1000 sccm. Thus, considering the limited number of measured flow rate, a proper discussion of this behavior is complex. However, note that we did not observe any noticeable variation of the sample surface temperature during the *nid* growth meaning that the density of active sites can be considered as constant whatever the gas flow rate. Considering the Harris and Goodwin reaction mechanisms [33,34] the influence of this latter one on hydrogen can thus be neglected. In such a simplified case, the figure 6 might be explained by a crossover between two regimes that are respectively limited by the mass transport and the surface reaction. At low flow rates (under around 100 sccm), the reactive hydrocarbon species reaching the sample surface increases with φ and speed up the growth following a square root law. Around 155 sccm, all the activated sites are saturated and the growth rate is no more dependent to φ.

The delay time Δt for each layer is displayed in Figure 7. One can see that its value strongly decreases with φ and drops to 0 under 1000 sccm (see also fig. 5), meaning that the transient regime is mostly governed by the "gas transit time". Indeed, the gas velocity v_{gas} in cm/s depends to the total gas flow rate *f* (in cm^3/min and proportional to φ) and the reaction chamber geometry. Δt can thus be expresses as:

$$\Delta t = \frac{\Delta l}{v_{gas}} = \frac{60\,\pi\,\Phi^2}{4f} \qquad (3)$$

with Φ (in cm) being the quartz tube diameter and Δl the distance between the sample and the gas injection point. Considering the tube section of 3.9 cm, a working pressure of 50 torr and a temperature in the quartz tube estimated around 40°C (temperature of the tube measured by a thermometer positioned inside the waveguide), a Δ*l* of 26.2 cm can be extracted from the experimental slope (1188 s.sccm). Being within 4% of the geometrical length (25.3 cm) measured on the reactor, this value confirms that this optical technique can be sensitive enough to follow gas transient regimes.

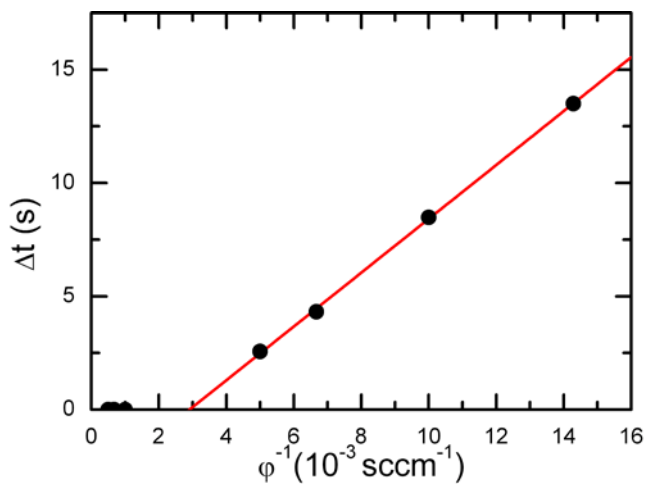

Figure 7. Transient regime Δt (extracted from fig. 4) as a function of the inverse of the gas flow rate.

4. Conclusion

In conclusion, we have shown that *in situ* Spectroscopic Ellipsometry is a powerful tool to extract real time values of the thickness and doping level of a diamond layer. The analysis of optical spectra, recorded during the growth, allowed us to reconstruct the doping profile of a metallic layer in good agreement with its SIMS measurement, thus confirming the accuracy of this optical characterization. Besides, by measuring the evolution of the transient regime of the growth of *nid* diamond layers under various gas flow rate we have been able to extract a value of the distance between the gas injection and the sample, very similar to the one measured on the reactor. These two experiments show that *in situ* spectroscopic ellipsometry can be a fast and non-destructive alternative to SIMS for the characterization of optical and electronic structures. By assessing the gas flow dynamic in the reactor, the doping profile of a layer and measuring in real time its growth rate and doping level, we have shown that *in situ* spectroscopic ellispometry is specially well-suited for the optimization of CVD processes and the exploration of new growth parameters.

References:

[1] T. Makino, S. Tanimoto, Y. Hayashi, H. Kato, N. Tokuda, M. Ogura et al., Diamond Schottky-*pn* diode with high forward current density and fast switching operation, Appl. Phys. Lett. **94** 262101 (2009)

[2] A. Nawawi, K. J. Tseng, Rusli, G. A. J. Amaratunga, H. Umezawa, and S. Shikata, Characterization of vertical Mo/diamond Schottky barrier diode from non-ideal I-V and C-V measurements based on MIS model, Diamond Relat. Matter. **35**, 1 (2013)

[3] H. Umezawa, Y. Kato, and S. Shikata, 1Ohm On-Resistance Diamond Vertical-Schottky Barrier Diode Operated at 250°C, Appl. Phys. Express, **6**, 011302 (2013)

[4] V. A. Kukushkin, M. A. Lobaev, D. B. Radischev, S. A. Bogdanov, M. N. Drozdov, V. A. Isaev et al., Bragg superlattices formed in growing chemically vapor deposited diamond, J. Appl. Phys. **120**, 224901 (2016)

[5] A. Fiori, J. Bousquet, D. Eon, F. Omnès, E. Bellet-Amalric and E. Bustarret, Boron-doped superlattices and Bragg mirrors in diamond, Appl. Phys. Lett. **105**, 081109 (2014).

[6] R. W. Collins, Y. Cong, Y.-T. Kim, K. Vedam, Y. Liou, A. Inspektor et al., Real-time spectroscopic ellipsometry characterization of diamond-like carbon, Thin Solid Films **181**, 565 (1989).

[7] R. W. Collins, Y. Cong, H. V. Nguyen, I. An, K. Vedam, T. Badzian et al., Real time spectroscopic ellipsometry characterization of the nucleation of diamond by filament-assisted chemical vapor deposition, J. Appl. Phys. **71**, 5287 (1992).

[8] Y. Hayashi, W. Drawl, R. W. Collins, and R. Messier, In-procces ellipsometric monitoring of diamond film growth by microwave plasma enhanced chemical vapor deposition, Appl. Phys. Lett. **60**, 2868 (1992).

[9] Y. Hayashi, X. Li, and S. Nishino, Ellipsometric monitoring of an oriented diamond nucleation process in bias-enhanced chemical vapor deposition, Appl. Phys. Lett. **71**, 2913 (1997).

[10] B. Hong, J. Lee, R. W. Collins, Y. Kuang, W. Drawl, R. Messier et al., Effect of processing conditions on the growth of nanocrystalline diamond thin films: real time spectroscopic ellipsometry studies, Diamond Relat. Mater. **6**, 1, 55 (1997).

[11] J. Lee, P. I. Rovira, I. An, and R. W. Collins, Rotating-compensator multichannel ellipsometry for characterization of the evolution of nonuniformities in diamond thin-film growth, Appl. Phys. Lett. **72**, 900 (1998).

[12] J. Lee, B. Hong, R. Messier, and R. W. Collins, Application of real-time spectroscopic ellipsometry for the development of low-temperature diamond film growth processes, Thin Solid Films 313–314, **506** (1998).

[13] E. Bustarret, F. Pruvost, M. Bernard, and C. Uzan-Saguy, Optical Conductivity Studies in Heavily Boron-Doped Diamond, Phys. Status Solidi A **186**, 303 (2001).

[14] E. Bustarret, E. Gheeraert, and K. Watanabe, Optical and electronic properties of heavily boron-doped homo-epitaxial diamond, Phys. Status Solidi A **199**, 9 (2003).

[15] S. Logothetidis, J. Petalas, H. M. Polatoglou, and D. Fuchs, Origin and temperature dependence of the direct gap of diamond, Phys. Rev. B, **46** :4483–4494, (1992).

[16] N. Kumagai, S. Yamasaki, and H. Okushi, Optical characterization of surface roughness of diamond by spectroscopic ellipsometry, Diam. Rel. Mat., **13**(11-12) :2092

[17] J. Bousquet, G. Chicot, D. Eon, and E. Bustarret, Spectroscopic Ellipsometry of homoepitaxial diamond multilayers and delta-doped structures, Appl. Phys. Lett. **104**, 021905 (2014).

[18] R. S. Balmer, I. Friel, S. M. Woolard, C. J. H. Wort, G. A. Scarsbrook, S. E. Coe et al., Unlocking diamond's potential as an electronic material, Philos. Trans. R. Soc., A **366**, 251 (2008).

[19] G. Chicot, A. Fiori, P. N. Volpe, T. Tran Thi, J-C. Gerbedoen, J. Bousquet et al., Electronic and physic-chemical properties of nanometric boron delta-doped diamond structures, J. Appl. Phys. **116**, 8, 083702 (2014)

[20] K. Ohno, F. J. Heremans, L. C. Bassett, B. A. Myers, D. M. Toyli, A. C. Bleszynski Jayich et al., Engineering shallow spins in diamond with nitrogen delta-doping, Appl. Phys. Lett. **101**, 082413 (2012)

[21] R. M. A. Azzam, N. M. Bashara, Ellipsometry and polarized light, North-Holland Publishing Co., Amsterdam (1977)

[22] N. Naka, K. Fukai, Y. Handa, and I. Akimoto, Direct measurement via cyclotron resonance of the carrier effective masses in pristine diamond, Phys. Rev. B, **88** 035205 (2013).

[23] H. Guyot, P. Achatz, A. Nicolaou, P. Le Fèvre, F. Bertran, A. Taleb-Ibrahimi et al., Band structure parameters of metallic diamond from angle-resolved photoemission spectroscopy, Phys. Rev. B, **92** :045135 (2015).

[24] M. Willatzen, M. Cardona, and N. Christensen, Linear muffin-tin-orbital and k.p calculation of effective masses and band structure of semiconducting diamond, Phys. Rev. B, **50**(24) :18054–18059 (1994).

[25] M. I. Eremets. Semiconducting diamond, Semiconductor Science and Technology, **6**(6):439 (1991).

[26] L. Reggiani, S. Bosi, C. Canali, F. Nava, and S. F. Kozlov, On lattice scattering effective mass of holes in natural diamond, Solid State Com. **30**(6) :333–335 (1979).

[27] P. Lawaetz, Valence-Band Parameters in Cubic Semiconductors, Phys. Rev. B, **4**(10) :3460–3467 (1971).

[28] J. Kono, S. Takeyama, T. Takamasu, N. Miura, N. Fujimori, Y. Nishibayashi et al., High-field cyclotron resonance and valence-band structure in semiconducting diamond, Phys. Rev. B, **48** 10917–10925 (1993).

[29] T. Klein, P. Achatz, J. Kacmarcik, C. Marcenat, F. Gustafsson, J. Marcus et al., Metal-insulator transition and superconductivity in boron-doped diamond, Phys. Rev. B, **75**(16): 165313 (2007)

[30] A. Kawano, H. Ishiwata, S. Iriyama, R. Okada, T. Yamaguchi, Y. Takano et al., Superconductor-to-insulator transition in boron-doped diamond films grown using chemical vapor deposition, Phys. Rev. B, **82**(8): 085318 (2010)

[31] J. Bousquet, T. Klein, M. Solana, L. Saminadayar, C. Marcenat and E. Bustarret, Phase diagram of boron-doped diamond revisited by thickness-dependent transport studies, Phys. Rev. B, **95**: 161301(R) (2017)

[32] J. Yu, R. Huang, L. Wen, C. Shi, Enhancement of HFCVD diamond growth process by directed gas flow, Mat. Lett., **32** (1997) 143-146

[33] J. E. Butler, R. L. Woodwin, Thin films diamond growth mechanisms, Philos. Transact. Royal Soc., **342**(1993):209-224

[34] D. G. Goodwin, Scaling laws for diamond chemical vapor deposition:Diamond surface chemistry, J. of Appl. Phys., **74**, 6888 (1993)